 doi:10.20944/preprints202203.0275.v1

Article

Study on CerAMfacturing of Novel Alumina Aerospike Nozzles by Lithography-based Ceramic Vat Photopolymerization (CerAM VPP)

Eric Schwarzer-Fischer [a,*], Johannes Abel [a], Jan Sieder-Katzmann [b], Martin Propst [b], Christian Bach [b], Uwe Scheithauer [a] and Alexander Michaelis [a]

[a] Fraunhofer IKTS, Winterbergstraße 28, 01277 Dresden
[b] Technische Universität Dresden, Helmholtzstr. 10, 01069 Dresden
* Correspondence: eric.schwarzer-fischer@ikts.fraunhofer.de; *Tel: +49-351-2553 7625*

Abstract: Advanced ceramics are recognized as key enabling materials possessing combinations of properties not achievable in other material classes. They are characterized by very high thermal, chemical and mechanical resistance and also usually have a lower density than metals. These properties predestine ceramics for many different applications, especially space applications. In the aerospace sector aerospike nozzles promise performance and application advantages compared to classic bell nozzles but are also inherently more complex to manufacture due to their shape. AM methods drastically simplify or even enable the fabrication of those complex structures while minimising the number of individual parts. The applicability of ceramic AM ("CerAMfacturing") on rocket engines and especially nozzles is consequently investigated in the frame of the "MACARONIS" project, a cooperation of the Institute of Aerospace Engineering at Technische Universität Dresden and the Fraunhofer Institute for Ceramic Technologies and Systems (IKTS) in Dresden. The goal is to develop novel large size aerospike thrust nozzles including areas of highest resolution and fineness. Finding a suitable AM process that enables the realisation of both aspects is extremely challenging. One possibility could be the hybridization of shaping methods, in that case CerAM VPP (ceramic additive manufacturing via vat photopolymerization) and CerAM FFF (ceramic additive manufacturing via fused filament fabrication) in combination with sinter joining. This contribution focuses on the high resolution CerAM VPP process, in particular the development, characterization and testing of a new photoreactive Al_2O_3 suspension validated by AM of novel aerospike nozzles.

Keywords: alumina; Additive Manufacturing (AM); CerAMfacturing; vat photopolymerization (VPP); digital light processing (DLP); Lithography-based Ceramic Manufacturing (LCM); cold-gas nozzle; aerospike nozzle

1. Introduction

Technical ceramics are among the most important high-performance materials in all fields of technology. In the aerospace section, the black and white heat protection tiles of the space shuttles are probably the best-known application [1]. Ceramic thermal barrier coatings in metallic rocket engines and turbines have also been established for many years. With additive manufacturing, there is now the possibility of opening completely new forms and fields of application for ceramic materials, as well as new potential for increasing performance and saving mass, which is required for aerospace application. One starting point, for example, would be the provision of a qualified cold-gas satellite thruster utilizing a ceramic nozzle for future space missions. While conventional engines are mainly made of metals - primarily copper for better heat transfer and nickel as a high-temperature resistant sheath - advanced ceramics are now also used as a construction material in these areas. Originally, ceramics were only applied as a thermal protection layer, e.g., in the Viking engine of Ariane 4 [2-5]. In the meantime, however, ceramic matrix

composites (CMCs: C/C, C/SiC, SiC/SiC, Al2O3/Al2O3 etc.) make it possible to build the entire engine from these lightweight materials. Schmidt et al [6], for example, were able to successfully test an uncooled rocket engine made of C/SiC for 8,900 s. In the field of AM of long fiber CMCs Abel et. al. investigated SiC/SiC composites manufactured by means of Fused Filament Fabrication [7]. By additive manufacturing, various monolithic or graded materials can be produced according to a pixel-by-pixel or line-by-line deposition or curing process. Depending on the principle of the layer building mechanism, not every ceramic powder can be processed. CerAM VPP (pixel-based) and CerAM FFF (line-based) are two representatives of CerAMfacturing and well-known AM processes for ceramic materials, for instance. These processes are known for ceramic materials but are comparatively young and already offer enormous design freedom today [8-10]. Within the MACARONIS project, a ceramic aerospike engine based on alumina is being designed, manufactured using additive processes and characterised under near-application conditions.

For this purpose, monolithic ceramic components made of alumina for operation below 1000 °C will first be additively manufactured and tested. The final goal is the hybridization of CerAM VPP and CerAM FFF to combine the advantages of both CerAM processes. Both are used to produce individual parts which are joined by sinter joining, a special joining process during sintering that does not require the use of strength-reducing additives. Sinter joining was developed and successfully patented at Fraunhofer [DE 10 2013 004 807 B4]. To enable hybridisation, the development of process-specific feedstocks (suspension for CerAM VPP and filaments for CerAM FFF) based on the same alumina powder was necessary. In this paper, only the developments in the field of CerAM VPP are described. The original stereolithography (SLA), invented by Charles W. Hull, is one of the best-known technologies compared to other AM processes and has been already used to produce ceramic green bodies based on alumina (Al_2O_3), silicon nitride, silica or for ZTA ceramics (zirconia toughened alumina) [11, 12]. The process is characterised by a photosensitive ceramic suspension, which initiates polymerisation through partial light exposure (often UV light), resulting in solidification of the material. The CerAM-VPP technology is derived from stereolithography and uses a digital light processing (DLP) module in combination with a digital micromirror device (DMD) for selective curing. One representative of the CerAM VPP technology, which is also used at the Fraunhofer IKTS, is the Lithography-based Ceramic Manufacturing (LCM) technology commercialized by Lithoz (Vienna, Austria) [9]. This technology works with a bottom-up approach and the selective photopolymerization of a highly particle-filled suspension by irradiation with blue light.

In this study the development of a photo reactive suspension for the CerAM VPP process based on an alumina, which was also used for the CerAM FFF process, is presented [13]. Therefore, three different monomer compositions were compared concerning their flow and curing properties, the printability and the quality of components after thermal processing. The suspension formulation with the best results was used for CerAM VPP of novel alumina aerospike thrusters with an engine size of 2.5 N and 10 N.

2. Materials and methods

The following section describes the utilized materials and methods, beginning with the general design process of the aerospike nozzles in the first section (2.1) and a comparison of two nozzle sizes. Subsequently (section 2.2 to 2.5) an overview regarding the raw materials, the suspension development including preparation and characterization and AM of test components, investigated by various methods, is given.

Preprints (www.preprints.org) | NOT PEER-REVIEWED | Posted: 21 March 2022 doi:10.20944/preprints202203.0275.v1

2.1 Design of novel aerospike nozzles

Aerospike nozzle designs for two thrust classes (2.5 N and 10 N) were derived using an in-house adaption of the nozzle design FORTRAN code of C. C. Lee [14]. The used design parameters for the supersonic contour of the nozzles are shown in **Error! Reference source not found.**.

Table 1. Aerospike nozzle design parameters.

design-parameter	2.5 N nozzle	10 N nozzle
throat gap	0.5 mm	1.0 mm
expansion ratio	2.93	2.93
design mass flow (GN2)	3.8 g/s	15.3 g/s
total pressure	203 kPa	203 kPa
nozzle pressure ratio	20.3	20.3

The main intention is to evaluate the suitability of the above-mentioned AM methods for their applicability for space application, especially in propulsion systems. Aerospike nozzles have been chosen, because they promise beneficial performance parameters in comparison to conventional bell nozzles in particular in launch system applications [15-19]. The performance advantage is based on a geometrically free gas expansion over a central body (spike) which allows the adaption of the expansion to ambient pressure. In conventional bell nozzles on the other hand, the supersonic expansion is defined by a fixed nozzle contour to a specific nozzle exit pressure, which causes performance losses in an off-design pressure scenario. With other words the efficiency of bell nozzles is depending on altitude.

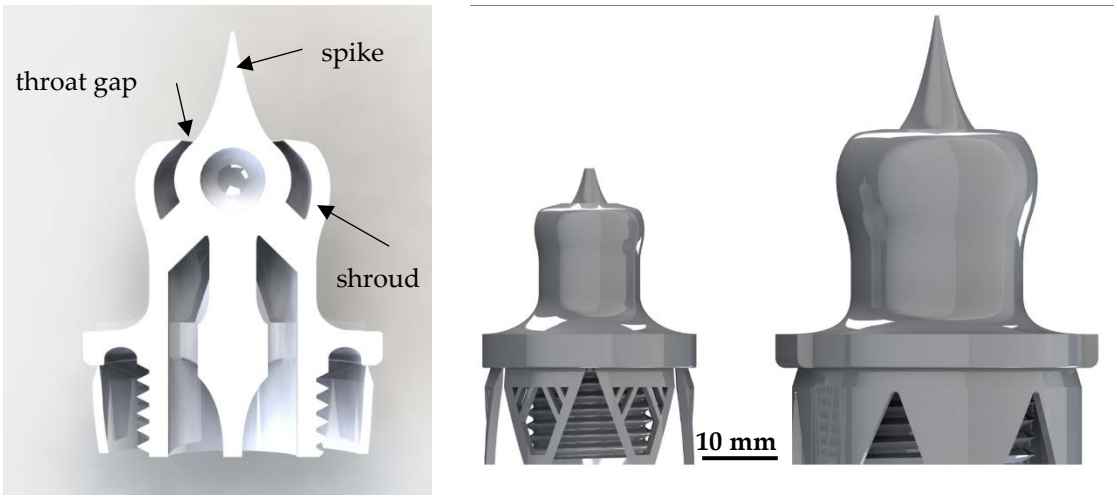

Figure 1: section display of an aerospike nozzle with needed support structures for AM (1) and size comparison of the 2.5N and the 10N cold-gas aerospike nozzle.

In this project, the aerospike nozzle (shown in Figure 1) is used in a cold-gas satellite thruster use-case to focus rather on the design, material and manufacturing challenges than on thermal management, which would become a dominant challenge in hot-gas applications. The key design and manufacturing challenges for the manufacturing can be summarized in the following requirements:

- Concentricity of the inner spike and the outer shroud (<25 µm)
- Dimensional accuracy and roundness of the annular throat gap (<20 µm)
- Low surface roughness (<20 µm)
- Cleanliness (no organic residues, no free particles)

Preprints (www.preprints.org) | NOT PEER-REVIEWED | Posted: 21 March 2022 doi:10.20944/preprints202203.0275.v1

In order to experimentally determine the flow characteristics and verify the design specifications of the fabricated nozzles, a test bench at TU Dresden is used, which is dedicated for measuring cold-gas nozzles. This test bench is situated in a vacuum chamber, which allows investigating higher pressure ratios between the feeding gas (up to 1.1 MPa) and the surrounding atmosphere (down to 5 kPa).

2.2 Raw materials and suspension development

As ceramic raw material alumina (AES-11C, $d_{0.5}$=0.4 µm, Sumitomo Chemical, Japan) with a BET-surface area of 7.66 m^2/g was used. The used dispersant was a solvent-free copolymer with acidic groups, especially a phosphoric polyester with pigment-affine groups usable for the stabilization of inorganic pigments (Altana AG, Germany). Various monomers with different functionalities were selected and evaluated regarding their performance. Three different resin compositions (rc) were tested as binder formulation, as can be seen in Table 2.

Table 2. components of the tested resin formulations with functionality and content in the mixture.

resin	components	functionality	viscosity	content [%]
rc1	• polyether acrylate	4	160 mPa*s	50
	• aliphatic urethane diacrylate	2	21 Pa*s	30
	• isobornyl methacrylate	1	12 mPa*s	20
rc2	• polyether acrylate	4	100 mPa*s	30
	• methylpentanediol diacrylate	2	9 mPa*s	20
	• butandiol monoacrylate	1	10 mPa*s	50
rc3	• amine modified polyester acrylate	1	150 mPa*s	40
	• acrylic acid ester	2	5 mPa*s	60

Camphorquinone was used as main photo initiator in combination with ethyl-4 dimethylamino benzoate as co-initiator (accelerator) to start the radical polymerization of the acrylates after exposure to visible light comparable to the light source of the printing device (wavelength λ=450-460 nm). Additionally, a polypropylene glycol (PPG, Sigma-Aldrich, USA) was used as plasticizing fluid to reduce the viscosity and the risk of defects due to thermal debindering. Based on the raw materials, photoreactive ceramic suspensions with an alumina powder content up to 50 vol.% were developed and prepared. At first, the photosensitive resin was prepared by mixing the monomers of the resin compositions (Table 2), the photo initiator with a content of 1 wt.% and the PPG with a content of 30 wt.% related to the resin by using a planetary centrifugal mixer (thinky ARV-310, C3-Prozess- und Analysentechnik, Germany) for 8 min at 2000 1/min. To achieve a complete dissolve of the initiator, a treatment of the premix in an ultrasonic bath was done followed by a second mixing step (8 min at 2000 rpm) in the planetary centrifugal mixer. Second, the dispersant and the alumina powder were added to the resin and mixed two times for 10 min at 2000 1/min with the planetary centrifugal mixer. As an intermediate step, the cup with the suspension was dissolved in an ultrasonic bath again for 5 min. The optimal dispersant content was investigated for rheological behavior and to achieve low suspension viscosity for the CerAM VPP process to manufacture high quality alumina components.

2.3 Suspension characterization

The quality of a CerAM VPP printed components is fundamentally determined by two essential properties of the used photosensitive suspension. On the one hand, this is the flow behavior, preferably determined by the shear viscosity, and on the other hand the light-induced polymerization of the suspension in dependence to its formulation and light energy used for curing.

 doi:10.20944/preprints202203.0275.v1

These two properties were quantified in more detail in order to derive suitable CerAM VPP parameters such as certain process speeds (e.g. vat rotation) as well as the required energy dose for exposure of one layer (generally 25 µm layer thickness).

The rheological properties were characterized by measuring the shear viscosity (Modular Compact Rheometer MCR302 with a cone/plate set-up, Anton Paar, Austria). Viscoelastic behavior (decreasing dynamic viscosity with increasing shear rates) in a low viscosity range (10 to 100 Pa*s at shear rates of 1-100 s^{-1}) is required for use with CerAM VPP, due to the rotational suspension coating mechanism of the process. The flow behavior, especially the dynamic viscosity, was measured by stressing the suspension with shear rates in a range of 0.1 to 1000 s^{-1}.

The curing by light exposure was determined by measuring the curing depth of a polymerized specimen (approx. 1 mL) depending on the suspensions formulation and the used energy dose (smart LED with 450-460 nm wavelength), a value resulting from the irradiation intensity with time (adjusted by a photometer). The layer thickness was measured by using a micrometer (High-Accuracy 13 Digimatic® Digital Micrometer). Afterwards, the necessary CerAM VPP process parameters were directly derived from the results.

2.4 Manufacturing of test components via CerAM VPP

Derived from the results of the suspension characterization, a set of processing parameters were used for the manufacturing of first test samples using the CeraFab 7500 printing device (Lithoz GmbH, Vienna, Austria). Within this process, a layer of the particle-filled slurry is applied by the rotation of a vat in combination with a static wiper blade. The bottom of the vat is transparent so the light source can locally expose the slurry from below. Using a dedicated optical system, the projected image is generated via a DMD with a resolution of 40 µm the xy-plane, which allow a minimum wall thickness of as low as 100 µm for sintered components. Achievable tolerances are in the range of 40-100 µm and known roughness are R_a values of 0.4 to 2 µm depending on powder type and part orientation.

As first test components small cubes and tubes were manufactured to evaluate the used printing parameters. Afterwards, bars (square cross-section of 5 mm edge size and length of 40 mm) and tubes (diameter d= 2 to 10 mm) were printed with the three different suspensions for comparison. Based on the results after thermal processing, more complex demonstrators, respectively the new designed aerospike nozzles were manufactured by using the most promising suspension. After printing, the green bodies are cleaned with a specific solution in combination with pressurized air. Following the common ceramic process chain, the green bodies undergo a debinding step to remove the polymers of the binder network and all organic compounds by heating them up to 600 °C in a nitrogen atmosphere using slow heating rates (4-10 K/h) with defined temperature holding levels (various dwell times in a range of 2-5 h) time. However, some carbon remains in the structure, that will be completely removed in a further tempering step up to 600 °C under air atmosphere. Sintering was done in air atmosphere by heating the components up to 1670 °C with a dwell time of 2 h. Heating rates of 1-3 K/min were used with a dwell time of 1 h at 600 °C and 1200 °C. Cooling down to 1200 °C was done with 0.5 K/min, followed by 1.5 K/min down to 40 °C.

2.5 Characterization of printed alumina components

After cleaning the printed test specimen, an initial green body inspection was carried out regarding the printing quality – general conditions, edges and surfaces. In a first analysis, the component quality for the three suspensions was compared to each other. For the most promising suspension, the debinding behavior was investigated in detail by thermogravimetric analysis (TGA, heating rate of 1 K/min; up to 900 °C). Based on the green

Preprints (www.preprints.org) | NOT PEER-REVIEWED | Posted: 21 March 2022 doi:10.20944/preprints202203.0275.v1

and sintered dimensions of the component, the sintering shrinkage and the shrinkage correction factors were determined as considered oversize to achieve the correct component dimensions (sintered state). Supporting the results of the sinter shrinkage of the most promising suspension, dilatometric measurements in xy- and z-direction were conducted (heating rate of 3 K/min; up to 1670 °C) for a detailed determination of the dimensional shrinkage.

The densities of the sintered samples were calculated by Archimedes principle using purified water. The relative densities of the samples were determined in relation to the theoretical density (ϱ_{th} = 3.92 g/cm³). The microstructure of the sintered tubes was captured by field emission scanning electron microscopy (FESEM, NVISION 40, Zeiss). The novel aerospike thrust nozzles were randomly checked concerning possible cracks or defects and other internal abnormalities by using computer tomography (CT Compact, 180kV – flat panel detector 5888x4600 pixel, Fa. Procon X-Ray, Sarstedt, Germany). The dimensional accuracy of the nozzles was also determined by 3D scans (ATOS core, GOM)

3. Results and discussion

Within this section, the results concerning suspensions development (3.1) including test component manufacturing (3.2) and characterizations (3.3) as well as the manufactured alumina aerospike nozzles (3.4) and its characterization (3.4, 3.5) are presented and discussed.

3.1 Suspension characterization

The Lithoz LCM technology as representative of the CerAM VPP process works with a light transparent vat, filled with a photosensitive ceramic suspension which is coated by a doctor blade to a thin layer. Standard thicknesses of the coated suspension have values between 100 to 400 µm, which lead to emerging shear rates up to approx. 2600 s^{-1} (100 µm layer thickness, 200 °/s vat rotation) all over the vat in dependence to vat rotation and coating thickness. Due to this, it is important and advantageously that the dynamic viscosity is homogeneous over the adjusted shear range. Figure 2 shows the dynamic viscosity in dependence to shear rate for the suspensions based on the three resin compositions compared to a reference (REF, Lithalox 350) [24].

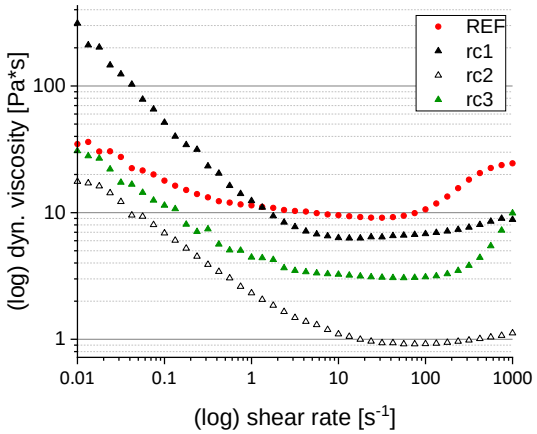

Figure 2. dynamic viscosity in dependence to shear rate; alumina suspensions with resin composition rc1, rc2 and rc3.

All three developed suspensions generally show a shear thinning behavior, but at different viscosity levels resulting from the different resin compositions. Resin composition rc1 shows the strongest decrease of viscosity changing within two decades by beginning at over 300 Pa*s down to 6 Pa*s^{-1} at low shear rates of 0.01 to 10 s^{-1}. Afterwards up to

Preprints (www.preprints.org) | NOT PEER-REVIEWED | Posted: 21 March 2022 doi:10.20944/preprints202203.0275.v1

1000 s^{-1} shear rate, the viscosity follows a nearly Newtonian behavior with 6-10 Pa*s. The behavior at low shear rates is not optimal for the described CerAM VPP process, as the resulting higher viscosity in the middle of the rotating vat as well as during the movement of the building platform (contact and detachment) leads to higher resistance forces, increasing the risk for damage of filigree component areas. Resin composition rc2 show the same viscosity behavior as resin composition rc1, but at a lower viscosity level ranging between 1-20 Pa*s for the entire shear range. The difference to rc1 is that rc2 consists only of low-viscosity monomers, whereas in rc1 a high-viscosity urethane acrylate is used. However, due to the much lower viscosity combined with a narrower range, the influence on the CerAM VPP process is much less compared to suspension formulation based on rc1. The low viscosity could be also unfavorable, as this reduces the wettability on the surface of the vat. The dewetting favors component defects due to lack of material. Additional additives such as surfactants could help to solve such upcoming phenomena. Resin composition rc3 in that case shows the best rheological behavior with a low viscosity over the whole shear range comparable to the commercial reference. This could be based to the medium viscosity of the monomers and the interaction between the functional groups to each other and with the surface charge of the alumina particles. Nevertheless, all three suspension formulations were processed in terms of the flow behavior in the CerAM VPP process.

A further important characteristic for a successful CerAM VPP processing is the curing behavior, which was analyzed here for all three suspensions. Therefore, the curing depth C_D of a suspension specimen was measured as function of energy dose. Based on the results the curing parameters for the CerAM VPP process were derived. Figure 3 shows the curing depth as function of energy dose for the three suspensions compared to the reference (REF).

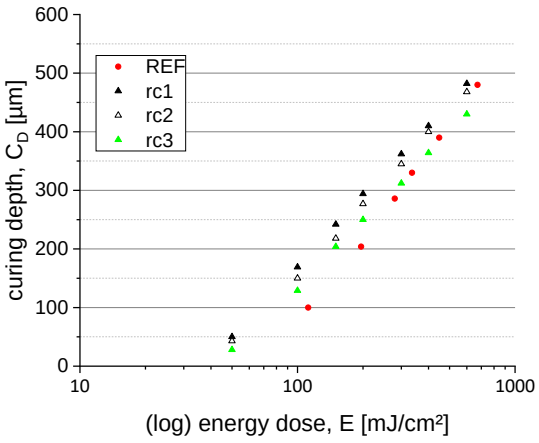

Figure 3. curing depth in dependence to energy dose; suspensions based on the resin composition rc1, rc2 and rc3.

In general, the cure depths of all three suspensions as well as the reference follow the Lambert-Beer´s law and forms as semi-logarithmic plot a straight line better known as "working curve" [20, 21]. There are only minor differences in the curing behaviors. In comparison to the reference, the developed suspensions have in that case a higher reactivity marked by the determined smaller critical energy dose (E_C) – the intersection of the straight lines with the x-axis. This means photolysis starts at a lower energy dose. The difference in the cure depth between the three resin compositions can be explained by the reactivity of the monomers. Due to the chemical structure of rc1, including a large amount of a high reactive tetrafunctional polyether acrylate, the reactivity is the greatest followed by rc2, including also a tetrafunctional polyether acrylate, but in a smaller amount and combined with a difunctional methylpentanediol diacrylate. As expected, the

 doi:10.20944/preprints202203.0275.v1

suspension based on rc3 shows the lowest reactivity visualized by the smallest critical energy dose and slope of the working curve since only a difunctional amine modified polyester acrylate is used. Achievable cure depths for all three formulations up to a maximum energy dose of 1000 mJ/cm² range between 450-480 µm, sufficient for the used CerAM VPP process, which normally works with a layer thickness of 25 µm. Based on the curing depth result, the energy dose for printing should be adjusted in a range of 50 to 130 mJ/cm² depending on the component design. Rough components with large exposure areas should be cured with lower energy dose, whereas filigree design with small wall thicknesses requires a higher energy dose.

3.2 Test components

After suspension development and characterization, initial printing tests were done by manufacturing cylindrical components with diameters of 4 mm to 12 mm. The printing parameter were set with a vat rotation of 200 °/s and an exposure energy dose of 75 mJ/cm² (rc1), 85 mJ/cm² (rc2) and 95 mJ/cm² (rc3). Figure 4 presents exemplarily printed and cleaned cylindrical green bodies as described.

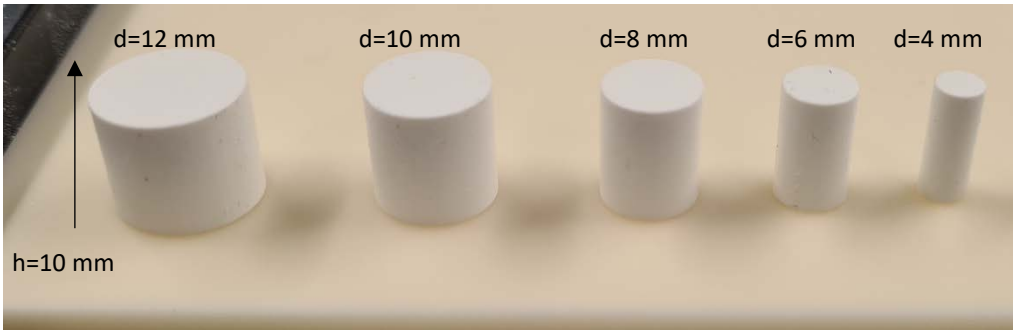

Figure 4. printed and cleaned cylindrical components; green state with various diameters and a height of h=10 mm.

Regardless of the resin composition, the three developed alumina suspension could be printed successfully with the adjusted parameters. After cleaning, the green cylinders were visual inspected for anomalies and possible defects, neither was not found. Following this initial quality inspection, the diameter and height of the cylinder were measured using a caliper. Actual value and target value matched quite well for all components, measured differences ranged within the tolerance of the caliper accuracy.

The next step in the process chain is the debinding, which was first done in nitrogen atmosphere, as it is known to be a much smoother for the components regarding crack formation. A slow heating rate of 10 K/h with a maximum debinding temperature of 600 °C and dwell times of 4 h every 100 °C was used. Figure presents exemplarily a choice of debinded cylinders.

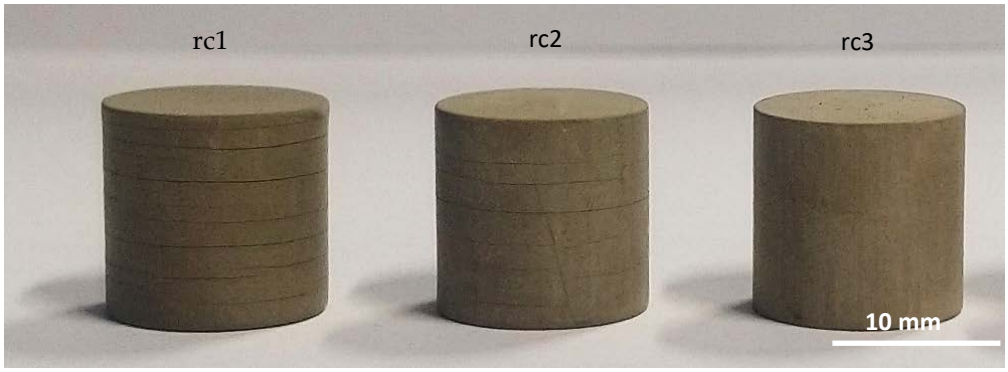

Figure 5. debindered cylinders (diameter d=12 mm) of all three developed suspensions.

Preprints (www.preprints.org) | NOT PEER-REVIEWED | Posted: 21 March 2022 doi:10.20944/preprints202203.0275.v1

As a result of the debinding, some cylinders showed significant cracking, especially those with a diameter of 12 mm. Furthermore, a kind of trend emerged, because the components based on rc1 had the most cracks followed by rc2 with only few cracks. Only the components of rc3 had no cracks formed during debinding. Based on this result and the moderate rheological behavior of rc3 suspension compared to the reference, it was decided to focus on this suspension for further steps. However, this does not mean that the other two formulations are unsuitable, but here it is imperative to investigate the debinding behavior more in detail to find the cause of the cracking and to have a chance to avoid crack formation in the future. After debinding the crack free cylinders were sintered in air atmosphere, the result is presented in Figure 6.

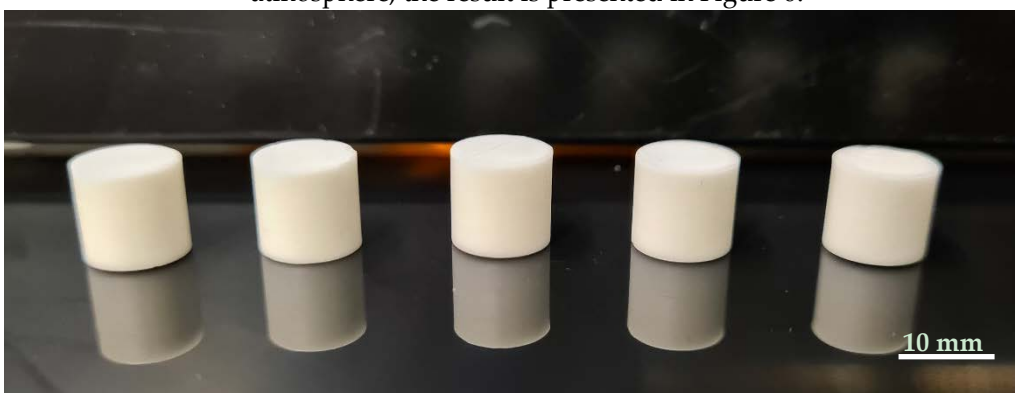

Figure 6. sintered alumina cylinders (d=12 mm) based on suspensionwith rc3.

As the result shows, the sintering of the cylindric test components with the used heating profile was successful, because no defects could be detected by visual inspection. Further characterizations such as density measurements and microstructure examinations were carried out in the next step and confirm the first good results.

3.3 Basic characterization

The first cylindrical test specimens were debinded very slowly for more than 120 h. A future goal is the optimization of debinding, especially the reduction of the debinding time without causing defects such as cracks. Therefore, the debinding of suspension based on monomer formulation rc3 were characterized more in detail by TGA. The result of the TGA is presented in Figure 7 as plot of weight loss ratio and weight loss in dependence to heating temperature.

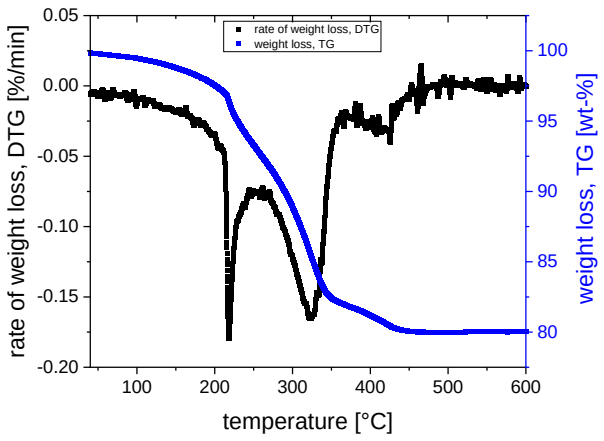

Figure 7. TGA – rate of weight loss and weight loss in dependence to heating temperature.

Preprints (www.preprints.org) | NOT PEER-REVIEWED | Posted: 21 March 2022 doi:10.20944/preprints202203.0275.v1

TGA analysis helps to understand the debinding and to find out how much of the binder monomers decompose at which temperatures. Based on the result it is possible to adjust and optimize the heating profile for remove of organics because a given TGA plot visualizes when and how much of them, especially of a certain component decompose. Depending on the formulation of the binder, different significant ranges (peak points) of decomposition occurs. For the used formulation rc3 a first gently zone occurs within 100 to 220 °C with a weight loss of up to 7 wt.% (of 21 wt.% complete binder), in that case the plasticizing fluid (PPG) decompose. This is one off the critical parts because the PPG starts to evaporate. If the heating rate is too high, in this stage the binder evaporation tends to crack formation, because the diffusion and pore formation is very slow due to the dense green body. The big (negative) increase of the weight loss rate shows the great danger of too much mass decomposition at too little space, in too short a time. It is necessary to heat up very gently up to 220 °C. After removing the PPG, a moderate pore space should be created which is advantageously for removing the other binder components. The next interesting range is within 270-320 °C, also marked by strong weight loss rate and a weight loss of 7-8 wt. %. Afterwards only a small range of low weight loss occurs at 380-420 °C with an uncritical weight loss of approx. 5 wt.%. Based on the given results, an optimized debinding profile with faster heating between the peak points were developed and used for the further manufactured test components.

The shrinkage behavior is not less important than the debinding, because on one side it is necessary to know about the dimensional shrinkage as oversize in all dimensions to achieve the correct components sizes after sinter shrinkage, and on the other side to know at which temperature and time the sinter shrinkage of the material occurs. The second point is very important for the sinter joining approach, an overall objective within the MACARONIS project. The shrinkage behavior must be known for all individual parts, which should be joined by sinter joining. By dilatometric measurements, the shrinkage in all dimensions were examined. In the next Figure 8, the result of the dilatometric measurement in xy- and z-direction is presented.

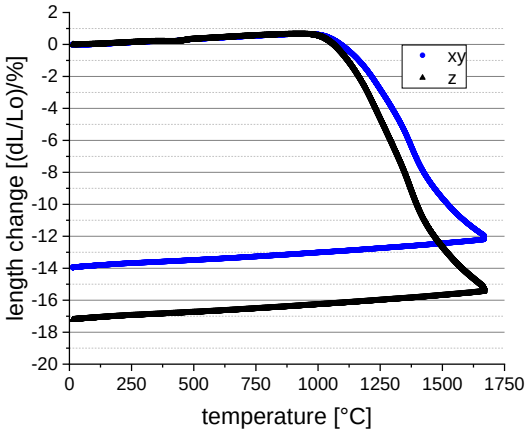

Figure 8. dilatometric measurements – temperature dependent shrinkage in xy- and z-direction of the CerAM VPP alumina.

As suggested, the results of the shrinkage measurements show a difference between the xy- and z-shrinkage, in that case a difference of 3 %. This phenomenon is known and seems to be a result of the layerwise building process. In general, the shrinkage values match to the expected values for the solid content of 50 vol.%. For dilatometry, debinded components have been used, so a debinding shrinkage of 3-4 % had to be added to the measured dilatometric shrinkage. In that case a total shrinkage of up to 18 % in xy-direction and up to 21 % in z-direction were estimated. To validate the results, the density of

Preprints (www.preprints.org) | NOT PEER-REVIEWED | Posted: 21 March 2022 doi:10.20944/preprints202203.0275.v1

the cylinders was measured by hydrostatic weighing with a value of 3.89 g/cm³, 99.3 % relative density compared to theoretical density of 3.92 g/cm³ for the used alumina.

Finally, the microstructure was analyzed by FESEM, and some images of the result are exemplarily shown in Figure 9.

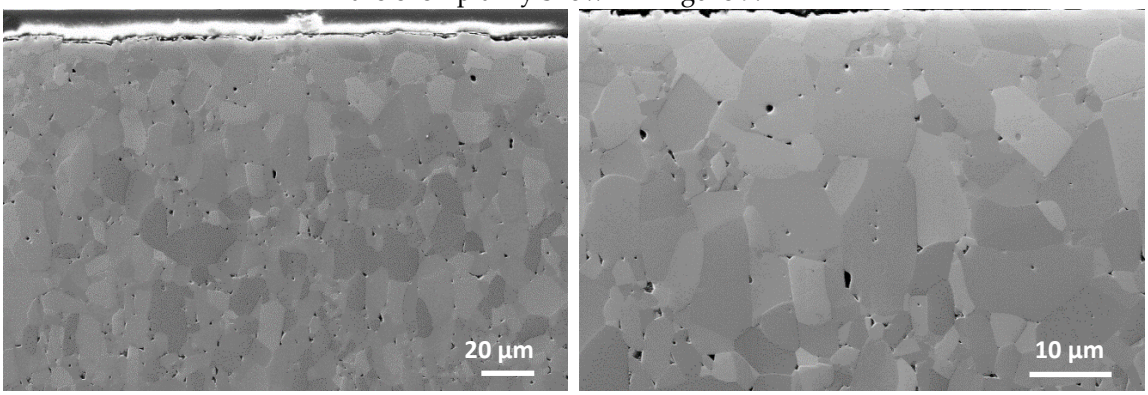

Figure 9. FESEM analyze of the CerAM VPP alumina microstructure, sintered at 1670 °C (2h dwell).

The result shows a microstructure with good quality, generally comparable to other shaping technologies for the used alumina material. The determined density is consistent with the microstructural images. The number of pores is manageable, but it could be even smaller in the future to achieve an even higher quality. Due to the sintering temperature of 1670 °C and dwell time of 2 h, partially a grain growth can be obtained as well as a decrease of grain interfaces marked by blurring and pores within large grains.

3.4 Novel alumina aerospike nozzles

After basic developments of the AES 11C-alumina material for CerAM VPP, test printing of the novel aerospike nozzles was performed. Therefore, the printing parameter, especially the layer curing energy was adjusted to the design. Due the fact that the sliced nozzle layers consist of small wall thicknesses with low exposure areas, the energy dose of the main layers were adjusted to approx. 100 mJ/cm². The first printing tests show a good result for the chosen parameter set in the green state. After debinding and sintering following the developed heating profile, a good component quality for the 2.5 N and 10 N nozzles was achieved as can be seen in Figure 10.

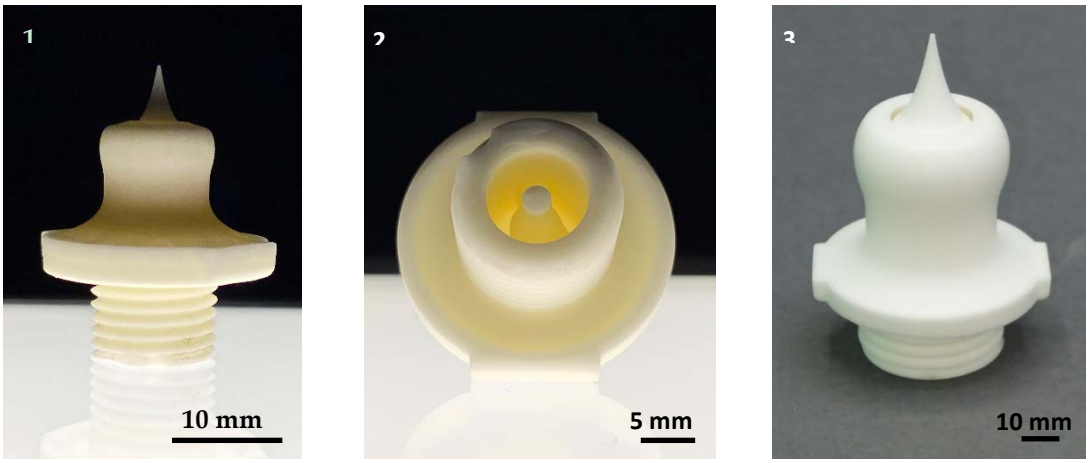

Figure 10. novel 2.5 N (1, 2) and 10 N (3) alumina nozzles additively manufactured by CerAM VPP technology.

After suspension development and parameter optimization, printing and thermal processing of novel alumina aerospike trust nozzles was successful. Components of high quality without visual cracks or any other fatal errors were achieved and the project goal

Preprints (www.preprints.org) | NOT PEER-REVIEWED | Posted: 21 March 2022 doi:10.20944/preprints202203.0275.v1

for single material AM of demonstrators can be positively concluded. The adjusted shrinkage correction as oversize factor for printing matches also very well because the fitting accuracy of the thread was given proved by screwing it into a socket with a corresponding metallic counter thread, as can be seen in Figure 11.

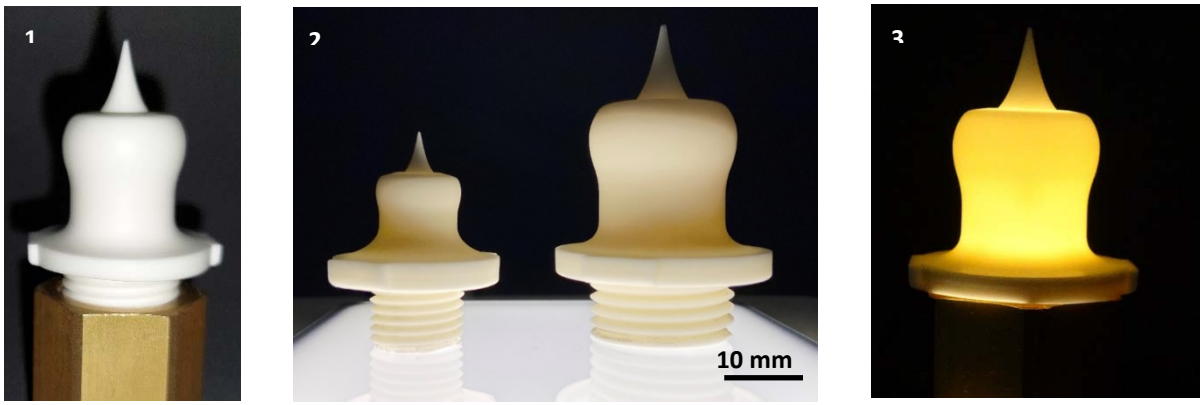

Figure 11. 10 N nozzle within a metallic counter thread (1); visualization of the size difference (2); transillumination by lamp for (large) defects (3) .

The thread of the nozzles can be fully screwed into the corresponding counter thread (for illustration purposes only it is shown in the half-screwed-in state). In the second image both nozzle sizes are compared to each other to illustrate the size differences and the third image shows a transillumination test with a lamp used as first simple check as screening for large cracks (have not been detected).

Since the two nozzle sizes shall be tested with regard to their functionality in a special test bench and for safety reasons, a non-destructive characterization for inner cracks and possible inhomogeneity were necessary and done by CT-analyses, two images of the cross section are exemplarily shown in Figure 13.

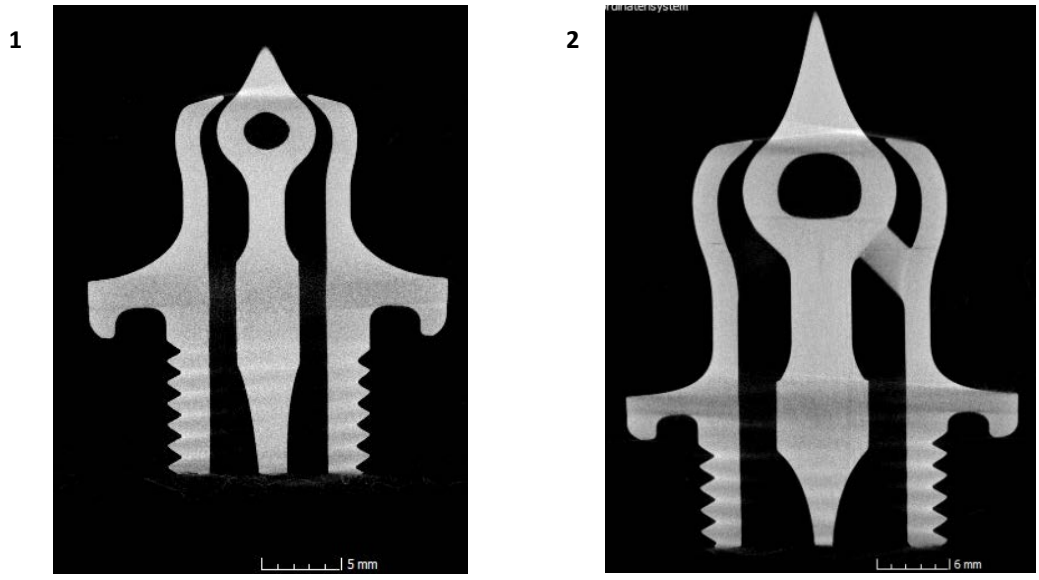

Figure 12. CT-images of 2.5 N (1) and 10 N (2) alumina nozzles.

Utilizing the CT-images, the result of transillumination by lamp could be confirmed, because no cracks or other anomalies were detected. Further, the images show the good quality of the nozzles in general and the surfaces as well as the well cleaned inner part.

 doi:10.20944/preprints202203.0275.v1

All channels are open, the narrow gap at the nozzle throat seem to be homogeneous and no essential errors were detected. With this result, the developed nozzles were ready for testing, which is currently being carried out at TU Dresden.

3.5 Experimental cold-gas and numerical flow characterization

The experimental determination of the flow characteristics and the verification of the design specifications of the fabricated nozzles are done by using a dedicated test bench. An exemplary test assembly is shown in Figure 13.

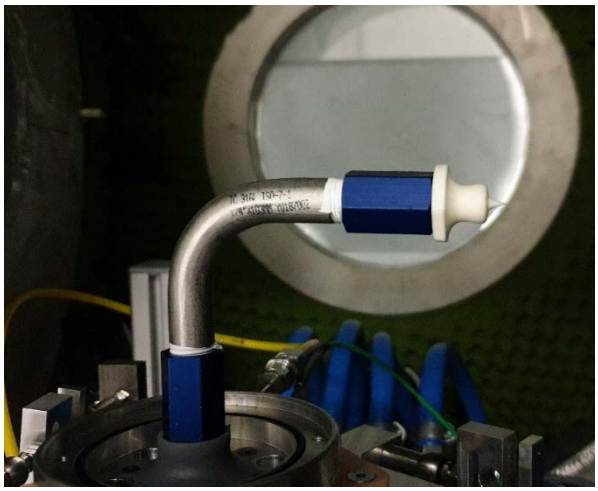

Figure 13. vacuum test bench for characterization of nozzle flow characteristics; equipped with 2.5 N nozzle.

A six-degree-of freedom force balance allows to measure simultaneously all three cartesian forces and torques, which allows in combination with the measured mass flow to evaluate the nozzle performance. The gas properties in terms of temperature and pressure are obtained close to the nozzle at in the nozzle holder, which also allows the calculation of the gas density [22, 23].

Numerical flow analyses utilizing ANSYS Fluent to solve the governing equations are used to investigate the influence of concentricity deviations and the effect of the surface roughness on the nozzle performance and the flow phenomena in otherwise nominal conditions. Deviations of the concentricity could result in a significant asymmetry of the pressure distribution on the nozzle surface, which itself causes undesirable side-forces that would have to be compensated. A high surface roughness on the other hand would cause a significant growth of the boundary layer of the flow. That increased boundary layer would act as a partial blocking of the nozzle throat and therefore reduce the mass flow and thrust performance of the nozzle. Hence, the numerical analyses serve as a fundament to evaluate and justify the quantification of the geometrical manufacturing requirements. Currently the additively manufactured 2.5 N and 10 N alumina nozzles are in examination with the test bench and the results will be presented in a subsequent publication.

4. Conclusion

Cold-gas aerospike nozzles based on alumina can be one opportunity to maneuver a new generation of satellites in space in the future. CerAMfacturing of novel designs for cold-gas satellite thruster with 2.5 N and 10 N trust is presented using CerAM VPP, a ceramic additive manufacturing technology based on stereolithography. For this purpose, the development of a novel photo reactive suspension based on alumina was necessary. Three tailored photo reactive monomer formulations were created and compared across

different properties after suspension preparation. The results show a strong influence of the monomers to the flow behavior, especially the dynamic viscosity influencing the CerAM VPP process directly. A further important effect of the binder formulation could be seen in the debinding results. The formulation is decisive for the success or failure of the debinding step. Strongly cross-linked polymers, which are made of highly functional monomers, have a higher tendency to form cracks. In this case, debinding must be carried out in a much more delicate and gentle manner to avoid the formation of defects. Both aerospike nozzles were manufactured by using suspension formulation based on resin composition rc3. Debinding as well as sintering led to ceramic nozzles of good quality. The measured density reached values above 99 % of the theoretical density which was confirmed using FESEM. In addition, the absence of defects in the nozzles were approved by means of computer tomography. All achieved results form a good basis for the next development step for instance, the hybridization of shaping methods to create larger nozzles. The approach is to combine components made by CerAM FFF as filament-based AM method with filigree CerAM VPP components of the same ceramic material via sinter joining without joining additives. This type of hybridization for such nozzles is currently under development. Detailed results will be presented in a following paper.

Acknowledgment: The authors acknowledge the funding of the Project MACARONIS (Manufactured Ceramic Aerospike Nozzle in Space, SAB, ILR - Ref.-Nr. 100376413; IKTS Ref.-Nr. 100376147) with EFRE funds by Sächsische Aufbaubank (SAB) gratefully.

References

[1] Lu, W.-Y. , Antoun, B. R., Korellis, J. S., Scheffel, S., Lee, M. Y., Hardy, R. D. and Costin, L. S.: "Material Characterization of Shuttle Thermal Protection System for Impact Analyses", Journal of Spacecraft and Rockets, 42 (5), 795-803 (2005)

[2] Wehner, F., "Application of an oxide-fibre-reinforced-oxide-ceramic (OCMC) for Rocket Combustion Chambers", Diploma thesis, Technische Universität Dresden, Faculty of Mechanical Science and Engineering (2014)

[3] Krenkel, W.: "Ceramic Matrix Composites", WILEY-VCH Verlag Gmbh & Co.KG, Weinheim (2008)

[4] Steyer T. E.: "Shaping the Future of Ceramics for Aerospace Applications", International Journal of Applied Ceramic Technology, 389-394 (2013)

[5] Bach, C.; Sieder, J.; Wehner, F., Nürmberger, M.; Przybilski, O. and Tajmar, M.: "Development and Verification of a 500 N Ethanol/LOX Rocket Engine using Oxide-Oxide Ceramic Matrix Composites", 6th European Conference for Aeronautics and Space Sciences (EUCASS), Kraków (2015)

[6] Schmidt, S., Beyer, S., Knabe, H., Immich, H., Meistring, R. and Gessler, A.: "Advanced ceramic matrix composite materials for current and future propulsion technology applications", Acta Astronautica, 55:409-420 (2004)

[7] Abel, J, Kunz, W., Michaelis, Mrityunjay, S., Klemm H.: "Non-oxide CMC fabricated by Fused Filament Fabrication (FFF)", J. Am. Soc., Vol 19, 2, pp.1148-1155, (2022), https://doi.org/10.1111/ijac.13944

[8] Abel, J., Scheithauer, U., Janics, T., Hampel, S., Cano, S., Müller-Köhn, A., Günther, A., Kukla, C., Moritz, T.: "Fused Filament Fabrication (FFF) of Metal-Ceramic Components", J. Vis. Exp., e57693 (2018)

[9] Homa, J.: "Rapid Prototyping of high-performance ceramics opens new opportunities for the CIM industry", PIM International, 6 (3), 65-68 (2012)

[10] Scheithauer, U. et al.: "Additive Manufacturing of ceramic heat exchanger - Opportunities and limits of the Lithography-based Ceramic Manufacturing (LCM)", JMEP (2017)
DOI: 10.1007/s11665-017-2843-z

[11] Griffith, M. L., Halloran, J. W.: „Freeform Fabrication of Ceramics via Stereolithography", J. Am. Ceram. Soc., 79 [10], 2601–2608, 1996.

[12] Licciulli, A. et al.: "Laser stereolithography of ZrO2 toughened Al2O3", J. Eur. Ceram. Soc., 24 [15–16], 3769–3777, (2004)

[13] Schwarzer-Fischer, E., Abel, J., Müller, F., Rebenklau, L., Barth, H., Alsdorf, N., Weingarten, S., Scheithauer, U. and Zins, M.: "Marriage of Technologies – Hybridization of Materials and Manufacturing Technologies for Ceramic Components", cfi/Ber. DKG 98, No. 5-6 (2021)

[14] Lee, C. C.: "Technical note R-41 - FORTRAN programs for plug nozzle design", Tech. Report BROWN Engineering Company (1963)

[15] Bach, C., Schöngarth, S., Bust, B., Propst, M., Sieder-Katzmann, J. and Tajmar, M.: "How to steer an aerospike", In 69th International As-tronautical Congress (2018)

[16] Hagemann, G., Immich, H. and Terhardt, M.: "Flow phenomena in advanced rocket nozzles - the plug nozzle", 34th AIAA/ASME/SAE/ASEE Joint Propulsion Conference and Exhibit, Joint Propulsion Conferences, July (1998)

[17] Hagemann, G., Immich, H., Nguyen, T. V. and Dumnov, G. E.: "Advanced rocket nozzles", Journal of Propulsion and Power, 14(5), September-October (1998)

[18] Kraiko, A. N. and Tillyayeva, N. I.: "Optimal profiling of the supersonic part of a plug nozzle contour", Fluid Dynamics, 35(6):945–955 (2000)

[19] Onofri, M., Nasuti, F., Calabro, M., Hagemann, G., Immich, H., Sacher, P. and Reijasse, P.: „Plug nozzles: Summary of flow features and engine performance", AIAA, 2002-0584 (2002)

[20] Jacobs, P. F.: "Fundamentals of Stereolithography", 3D Systems Inc., 196–211 (1992)

[21] Griffith, M.L., Halloran, J.W.: "Freeform Fabrication of Ceramics via Stereolithography", J. Am. Ceram. Soc., 79 (10), 2601–2608 (1996)

[22] Sieder-Katzmann, J., Propst, M., Tajmar, M., Bach, C.: **"**Cold gas experiments on linear, thrust-vectored aerospike nozzles through secondary injection", In 70th International Astronautical Congress, Washington D.C., USA (2019)

[23] Sieder-Katzmann, J., Propst, M., Tajmar, M., Bach, C.: "Investigation of aerodynamic thrust-vector control for aerospike nozzles in cold-gas experiments", In Space Propulsion Conference 2020+1. Virtual Conference (2021)

[24] Lithoz GmbH → Slurry Data Sheet SDS 201.71, LithaLox 350, V 7 ISSUE DATE: 03.07.2019